JGR Atmospheres

RESEARCH ARTICLE
10.1029/2023JD039207

Tropical Pacific Modulation of the Asian Summer Monsoon Over the Last Millennium in Paleoclimate Data Assimilation Reconstructions

Jun Hu[1], Sylvia Dee[2], Grant Parajuli[2], and Kaustubh Thirumalai[3]

[1]College of Ocean and Earth Sciences, Center for Marine Meteorology and Climate Change, Xiamen University, Xiamen, China, [2]Department of Earth, Environmental, and Planetary Sciences, Rice University, Houston, TX, USA, [3]Department of Geosciences, University of Arizona, Tucson, AZ, USA

Key Points:

- The El Niño-Southern Oscillation (ENSO) teleconnections to the Asian summer monsoon have evident decadal-to-centennial variability in the last 1,000 years
- During most of the last 1,000 years, El Niño tends to be associated with weak Asian summer monsoon rainfall
- Weak ENSO-East Asian summer monsoon teleconnection is associated with sea surface temperature anomalies resembling El Niño events

Supporting Information:

Supporting Information may be found in the online version of this article.

Correspondence to:

J. Hu,
hujun@xmu.edu.cn

Citation:

Hu, J., Dee, S., Parajuli, G., & Thirumalai, K. (2023). Tropical Pacific modulation of the Asian summer monsoon over the last millennium in paleoclimate data assimilation reconstructions. *Journal of Geophysical Research: Atmospheres*, *128*, e2023JD039207. https://doi.org/10.1029/2023JD039207

Received 4 MAY 2023
Accepted 22 SEP 2023

Abstract Large uncertainties exist in climate model projections of the Asian summer monsoon (ASM). The El Niño-Southern Oscillation (ENSO) is an important modulator of the ASM, but the ENSO-ASM teleconnection is not stationary. Furthermore, teleconnections between ENSO and the East Asian versus South Asian subcomponents of the ASM exhibit distinct characteristics. Therefore, understanding the variability of the ENSO-ASM teleconnection is critical for anticipating future variations in ASM intensity. To this end, we here use paleoclimate records to extend temporal coverage beyond the instrumental era by millennia. Recently, data assimilation techniques have been applied for the last millennium, which facilitates physically consistent, globally gridded climate reconstructions informed by paleoclimate observations. We use these novel data assimilation products to investigate variations in the ENSO-ASM relationship over the last 1,000 years. We find that correlations between ENSO and ASM indices are mostly negative in the last millennium, suggesting that strong ASM years are often associated with La Niña events. During periods of weak correlations between ENSO and the East Asian summer monsoon, we observe an El Niño-like sea surface temperature (SST) pattern in the Pacific. Additionally, SST patterns associated with periods of weak correlations between ENSO and South Asian summer monsoon rainfall are not consistent among data assimilation products. This underscores the importance of developing more precipitation-sensitive paleoclimate proxies in the Indian subcontinental realm over the last millennium. Our study serves as a baseline for future appraisals of paleoclimate assimilation products and an example of informing our understanding of decadal-scale ENSO-ASM teleconnection variability using paleoclimate data sets.

Plain Language Summary A large fraction of floods and droughts in Asia are associated with extreme Asian summer monsoon (ASM) events, but unfortunately, the prediction of the ASM is still highly uncertain. Scientists often use El Niño—warm sea surface temperature (SST) events in the eastern Pacific Ocean that occur before the ASM—as a basis to predict the ASM, but it does not work perfectly all the time. In order to understand why El Niño fails to predict the ASM sometimes, we looked at climate data spanning the last 1,000 years. The data was based on paleoclimate reconstructions using archives including tree rings, corals, speleothems, and ice cores. Scientists recently synthesized all these data together with climate model simulations. We find that more intense summer monsoon rainfall in East and South Asia likely corresponds to colder SSTs in the Eastern Pacific Ocean. Also, when El Niño fails to predict the monsoon in East Asia, the background SST in the eastern Pacific is warmer than normal. Our results could help better predict ASM rainfall in the future and mitigate impacts of fire and flooding caused by extreme monsoon events.

1. Introduction

The Asian summer monsoon (ASM) supplies freshwater resources for nearly 4 billion people annually. Its variations and related hydroclimate events cause floods and droughts, which have far-reaching social and economic impacts, especially in countries that are heavily dependent on agriculture (Gadgil & Kumar, 2006; Loo et al., 2015; Wang et al., 2022). Climate change is expected to change the characteristics of the ASM (Rajesh & Goswami, 2022); dry and hot monsoon extremes are expected to occur more frequently alongside future warming (Mishra et al., 2020), in addition to the increased risk of flash flooding (Almazroui et al., 2021). Given its societal and climatic importance, it is critical to constrain the future response of ASM variability to anthropogenic forcing. Ensemble means of the Coupled Model Intercomparison Project Phase 3 (CMIP3), CMIP5, and CMIP6

projections suggest a robust increase of ASM rainfall under increased greenhouse gas scenarios, but significant spread in spatial extent and magnitude between these model simulations adds marked uncertainty to anticipating future ASM variability (Ha et al., 2020; Katzenberger et al., 2021; Lee & Wang, 2014; Menon et al., 2013; Sooraj et al., 2015).

Variations in sea surface temperature (SST) in the tropical Pacific Ocean play an outsized role in influencing ASM fluctuations from year to year. Chiefly, the El Niño-Southern Oscillation (ENSO) phenomenon is an important predictor of the ASM: the amplitude or variance of ENSO can modulate the magnitude of the ASM via teleconnections (Xie et al., 2016). The ASM has two major subsystems, the South Asian summer monsoon (SASM) and the East Asian summer monsoon (EASM). Whereas the SASM is a tropical monsoon system, the EASM is a subtropical monsoon system and is influenced by tropical circulation and midlatitude systems such as extratropical cyclones and westerly jet streams (Lau et al., 2000; Wang et al., 2001). Thus, the two subsystems respond to ENSO differently. For example, typically during El Niño events, rainfall generally decreases in the SASM realm (Nanjundiah et al., 2013), whereas monsoon rainfall is enhanced in southern China (Dai & Wigley, 2000).

ENSO often influences the EASM and SASM by triggering SST responses in the Indian Ocean or by modulating changes in the Walker Circulation (Zhou et al., 2021). ENSO peaks in boreal winter (December-January-February; DJF), but the ENSO-monsoon teleconnection propagates into the following boreal summer season (June-July-August; JJA). The Indian Ocean connects ENSO to the ASM via the Indian Ocean Basin mode (IOB) and the Indian Ocean Dipole (IOD) (Cherchi et al., 2021; Liu & Duan, 2017; McMonigal & Larson, 2022). In boreal autumn, El Niño weakens the Walker circulation, and this triggers the positive phase of the IOD (Schott et al., 2009). In winter, El Niño induces a large-scale anomalous cyclone (AC) in the central Pacific and an anomalous anticyclone (AAC) to the west (Wang et al., 2003). In the tropical Indian Ocean, the easterly wind anomalies excite downwelling Rossby waves in the southern tropical Indian Ocean, resulting in warming in the southwest Indian Ocean (Xie et al., 2002). This warming is maintained by air-sea interactions and transitions into IOB warming through boreal summer following El Niño (Du et al., 2009). In spring and summer, the IOB warming excites Kelvin waves in the lower atmosphere and thus strengthens the AAC over the northwestern Pacific, weakening the SASM circulation and strengthening the EASM (Xie et al., 2009). In addition, the positive phase of IOD triggered by El Niño can induce convergence anomalies in India, reducing the ENSO-induced rainfall deficit in India (Ashok et al., 2001).

Broadly, multiple hypotheses explaining the variation of the ENSO-monsoon relationship have been proposed which draw from this mechanism, including atmospheric/oceanic wave propagation and air-sea interactions. However, the ENSO-monsoon relationship is not inherently stable and exhibits substantial decadal variability (Kumar et al., 2006; Kumar, Kleeman, et al., 1999; Torrence & Webster, 1999; Wang, 2002; Wu & Wang, 2002). Indeed, the variation of the ENSO-monsoon relationship is likely modulated by external forcings such as solar irradiance (Mehta & Lau, 1997; Misios et al., 2019), insolation (Wen et al., 2022), greenhouse gases (GHGs) (Ashrit et al., 2001; Li & Ting, 2015), and aerosols (Khodri et al., 2017; Singh et al., 2020). ENSO-monsoon teleconnections are also modulated by internal modes of climate variability such as the Pacific Decadal Oscillation (PDO) (Chan & Zhou, 2005; Dong et al., 2018; Krishnamurthy & Krishnamurthy, 2014) and the Atlantic Multidecadal Oscillation (AMO) (Kucharski et al., 2009; Lu et al., 2006). Other work suggests that decadal variability of the ENSO-monsoon relationship is simply caused by stochastic perturbations rather than low-frequency deterministic processes (Cash et al., 2017; Gershunov et al., 2001; Yun & Timmermann, 2018), and that internal modes such as PDO are induced by stochastic processes (Newman et al., 2016). Exacerbating the lack of constraints on the ENSO-monsoon relationship, there are only 3–4 full cycles of decadal variability with which to characterize the ENSO-monsoon relationship over the instrumental period.

Over the instrumental period, strong El Niño events usually coincide with the failure of the SASM (i.e., drought events in the core monsoon zone of India). Given that ENSO events modulate SASM activity during JJA of the following year—well after they peak in DJF—ENSO indices have been used as predictors for the monsoon (Nanjundiah et al., 2013). The super El Niño event in 1997/1998 seems to be an outlier: it features an extremely warm SST anomaly in the central and eastern Pacific but corresponds to a slight *increase* of SASM rainfall. Several hypotheses have been raised to explain this anomalous event: Kumar, Rajagopalan, & Cane (1999) suggested that the ENSO-monsoon teleconnection has weakened in recent decades such that the slight increase in SASM rainfall following the 1997/1998 El Niño event could represent this decoupling. Nanjundiah et al. (2013) suggested that central equatorial Indian Ocean SSTs may be another important factor, and they are not always

in phase with ENSO. Nevertheless, there are only three super El Niño events in 1952–2010 (defined as events with the Nino3 index exceeding two standard deviations, i.e., events in 1972/1973, 1982/1983, and 1997/1998) (Hong et al., 2014); thus, we lack the sample space to robustly characterize the ENSO-SASM relationship. For EASM rainfall, evidence exists for a shift in its relationship with ENSO from 1960s to 1990s (Wang, 2002; Wu & Wang, 2002). Although several factors including the North Atlantic Oscillation (Wu, Li, Jiang, He, & Zhu, 2012), Tibetan Plateau snow cover (Wu, Li, Jiang, & Ma, 2012), PDO (Chan & Zhou, 2005), and AMO (Lu et al., 2006) have been invoked as possibly responsible for the decadal shift of the ENSO-EASM teleconnection, understanding the mechanisms for this are still challenging due to the brevity of the instrumental period.

Paleoclimate records extend the temporal coverage afforded by the instrumental era, and several studies have investigated the ENSO-monsoon relationship spanning the last millennium and the Holocene (Abram et al., 2007; Berkelhammer et al., 2014; Eroglu et al., 2016; Liu et al., 2018; Tejavath et al., 2019; Yan et al., 2015; Zhang et al., 2018). Many of these studies highlight decadal-to-centennial-scale variability of the ENSO-monsoon relationship (e.g., difference between the Little Ice Age and the Medieval Warm Period) and the important roles of the PDO and AMO. However, most of these studies are generally based on one or a few paleoclimate records or sites, limiting ability to capture the spatial heterogeneity of the ASM's response to ENSO. Accordingly, validation of model-specific spatial heterogeneity, which may be sizable across models (Liu et al., 2018; Tejavath et al., 2019; Zhang et al., 2018), necessitates quantitative information of climate evolution afforded by paleoclimate records. Addressing these limitations, recent efforts to amalgamate and standardize global paleoclimate data sets have advanced paleoclimate synthesis (Hakim et al., 2016; Steiger et al., 2018). The past two millennia emerge as a promising period of study due to well-constrained global climatic forcing factors (Schmidt et al., 2011) and good coverage of proxy information (Steiger et al., 2018; Tardif et al., 2019a). As such, a number of recent paleoclimate data assimilation products have focused on the last two thousand years (1–2000 C.E.; Last2k) to provide model-blended global reconstructions of surface temperature and precipitation (Hakim et al., 2016; Steiger et al., 2018). Such paleoclimate data assimilation techniques facilitate physically consistent, globally gridded climate reconstructions informed by paleoclimate observations within the dynamical constraints of climate models.

To improve understanding of the dynamics of the ASM, here, we focus on the relationship between ENSO and the ASM over the last 1,000 years. We use two state-of-the-art data assimilation-based paleoclimate reconstructions, the Last Millennium Reanalysis (LMR) (Tardif et al., 2019a) and the Paleo-Hydrodynamics Data Assimilation (PHYDA) (Steiger et al., 2018), which both contain information surrounding ENSO and hydroclimate in the ASM core regions. We address three key questions: (a) How does the ENSO-ASM relationship change over the last millennium? (b) Do historically observed ENSO-monsoon teleconnection relationships hold in the past? and (c) What are the dynamics associated with periods of strong and weak ENSO-ASM teleconnections? We discuss the utility of these results to form testbeds for numerical models, and to better understand the background climate states associated with periods of strong and weak ENSO-ASM teleconnections.

2. Data and Methodology

2.1. Paleoclimate Data Assimilation Reconstructions

The Last Millennium Reanalysis (LMR) project v2.0 (Tardif et al., 2019a) uses offline Data Assimilation (DA) with a climate model prior derived from simulations spanning the last millennium (Landrum et al., 2013) in combination with annually resolved paleoclimate archives from the PAGES2k database (Emile-Geay et al., 2017) (with later additions from Anderson et al. (2019) and Tardif et al. (2019a)). The DA employs an ensemble Kalman filter to reconstruct annual climate states which minimize the offset between model fields (the model "prior") and observations (Hakim et al., 2016; Steiger et al., 2014; Tardif et al., 2019a). The result is an annually resolved reconstruction of fields including (but not limited to) SST, surface air temperature, precipitation, the Palmer Drought Severity Index (PDSI), and geopotential height. The LMR has a spatial resolution of $2° \times 2°$, covering the period 1–2000 C.E., and reconstructs climate averaging over the calendar year beginning in January and ending in December.

The Paleo-Hydrodynamics Data Assimilation product (PHYDA) combines 2,978 proxy time series with the physical constraints of climate models, using a similar DA framework to the LMR (Steiger et al., 2018). PHYDA returns climate state variables at seasonal to annual resolution including two-dimensional fields PDSI,

Standardized Precipitation Evapotranspiration Index (SPEI), and surface temperature. Climate indices for the AMO, NAO, ENSO, and several others are also provided in the reconstruction. Note that PHYDA does not reconstruct precipitation. PHYDA has a spatial resolution of 1.875° (latitude) × 2.5°(longitude), and covers the period 1–2000 C.E. Unlike the LMR, PHYDA's annual reconstructions average over the water year, from April to March. PHYDA employs proxy records from the PAGES2k proxy database (Emile-Geay et al., 2017), but screens for and includes only hydroclimate-sensitive proxy archives such as tree-ring width, as described in Steiger et al. (2018). The available reconstructions of climate modes and their hydroclimatic impact from PHYDA facilitate the investigation of the past influences and interactions between ENSO and the ASM.

Both LMR and PHYDA employ data assimilation techniques to combine the information in paleoclimate proxies with the dynamical constraint of a climate model, so LMR and PHYDA provide physically coherent global climate variables relevant to this analysis, including SST, air temperature, precipitation, and sea level pressure spanning the last 2000 years at annual resolution. These products provide a complement to direct measurements from paleoclimate archives, as they effectively fuse information contained in the high-resolution paleoclimate record with the dynamical constraints of a climate model (Dee et al., 2016; Steiger et al., 2014); PHYDA and LMR thus "fill in the gaps" in time and space where data points are lacking in paleoclimate records (Hakim et al., 2016; Tardif et al., 2019a).

The proxy network and data assimilation techniques employed in the LMR and PHYDA house similarities, but there are also important differences. First, the two products use different climate model priors. PHYDA used the Community Earth System Model Last Millennium Ensemble (CESM-LME) (Otto-Bliesner et al., 2016), whereas the LMR used the Last Millennium simulation from the Community Climate System Model version 4 (CCSM4) (Landrum et al., 2013). Furthermore, the prior used in PHYDA (CESM-LME) was bias-corrected to observations, whereas the LMR framework applied no bias-correction. In terms of the proxy network, though both LMR and PHYDA assimilate the PAGES 2k proxy data collection (Emile-Geay et al., 2017), PHYDA also includes the tree-ring width collection of Breitenmoser et al. (2014) and other 59 publicly available proxy records including ice cores, speleothems, and lake sediments (Steiger et al., 2018). Therefore, the LMR and PHYDA are structurally dissimilar; the evaluation of both data assimilation products in this study is geared toward identifying robust ENSO teleconnection signals that emerge no matter the choice of proxy network or model prior. Finally, as a cross-check of the PHYDA and LMR results against the model priors, we performed similar analyses with the CESM-LME simulations.

We note proxy data availability for the first 1,000 years of the Common Era is limited, and therefore we analyze only the data over the last millennium (1,000–2,000 C.E.) from the LMR and PHYDA in this study.

2.2. Validation Data

We validate the spatial patterns of PDSI in the LMR and PHYDA against the observation-derived PDSI produced by Dai (2011). The data set from Dai (2011) ("Dai data set" in the text that follows) reconstructs PDSI based on observed monthly precipitation and temperature globally on a 2.5° latitude/longitude grid from 1850 to 2018. We also use precipitation from the Global Precipitation Climatology Center (GPCC) (Becker et al., 2013) to validate precipitation in the LMR. The GPCC data set provides gridded gauge-analysis precipitation products derived from quality-controlled station data with a 2.5° latitude/longitude grid from 1891 to the present.

2.3. ENSO and ASM Definitions

We obtain time series of both ENSO and the intensity of the East Asian and South Asian summer monsoons using SST, precipitation, and PDSI in the DA products.

To calculate the intensity of the Asian monsoon in the past, we employ a suite of published monsoon indices. While some index methods place emphasis on circulation patterns (Wang et al., 2008; Wang & Fan, 1999), others focus on metrics of rainfall intensity (Goswami et al., 2006; Tao & Chen, 1987). In the paleoclimate realm, high-resolution, well-dated proxies such as tree rings and speleothems often are sensitive to moisture availability or rainfall, but there are few high-resolution proxies for wind; thus, we focus on indices employing rainfall amount. For the EASM, the index is defined as the summer rainfall between 27°N and 35°N and 105°−125°E (Wang et al., 2008). The index for the SASM is defined by the summer rainfall between 18°N and 25°N and

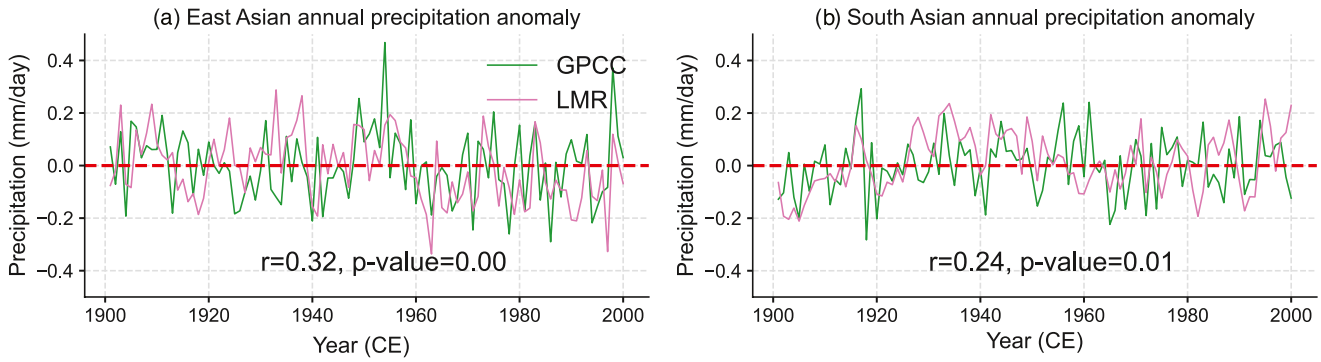

Figure 1. Time series of the East Asian (a) and South Asian (b) precipitation anomalies from 1900 to 2000, calculated from the Global Precipitation Climatology Center (GPCC) (green) and Last Millennium Reanalysis (LMR) (magenta) data sets. The correlations between the GPCC and LMR time series together with corresponding *p* values are annotated at the bottom of each panel.

65°−88°E (Rani et al., 2021) (Figure S1 in Supporting Information S1). Because PHYDA uses calendar years beginning in April and ending in March, we calculate averages using April-March monthly intervals in corresponding observational data when conducting validation for PHYDA.

We use the NINO3.4 index to evaluate ENSO variability in these products, as its relationship with the ASM over the instrumental era is well studied (see Section 1). The NINO3.4 index is calculated as the averaged SST anomaly between 5°S−5°N and 170°−120°W.

We calculate the correlation between ENSO and the Asian monsoon indices using a 30-year moving window for all years across the last millennium. We opt for a 30-year window size, which strikes a balance between ample degrees of freedom and capturing interannual variability rather than decadal variability. (Note that as shown in Section 3.3, the choice of window size does not influence our results). Variation in this correlation highlights periods where the ENSO-monsoon relationship is robust (statistically significant) or when the relationship is weak (insignificant). Weak ENSO-monsoon teleconnection periods are defined as years when the absolute values of the correlation coefficients (R) are smaller than the tenth percentile of the absolute value of all correlation coefficients (i.e., $0 < |R| <$ tenth percentile ($|R|$)); strong ENSO-monsoon teleconnection periods are defined as years when the correlation coefficient R is less than the tenth percentile of all correlation coefficients ($R <$ tenth percentile (R)), highlighting years when the correlation is strongly negative. Finally, we examine the periodicities associated with high ENSO-monsoon correlations.

3. Results

3.1. Paleoclimate Data Assimilation Product Validation

We first compare the statistics of rainfall in PHYDA and LMR to observations from the 20th-century instrumental period to (a) determine whether these two products accurately capture ASM rainfall, and (b) in order to quantify biases. Figure 1 shows the time series of regionally-averaged East (Figure 1a) and South (Figure 1b) Asian precipitation from 1901 to 2000 for the LMR and the GPCC data set. The correlations between the assimilation product LMR and observed GPCC precipitation over the Asian monsoon regions are significant at the 95% level. Similarly, correlations between PDSI reconstructed in the LMR and PHYDA and observation-derived PDSI (Dai, 2011) are significant at the 95% level (Figure 2). Figure 2 indicates that correlation coefficients (data assimilation reconstruction vs. observations) are higher for the LMR in all cases compared to PHYDA (R values are annotated in Figures 1 and 2). Since PHYDA PDSI is averaged over April-March (the water year), we also recalculated the Dai PDSI index over April-March water years, and confirmed the correlation coefficients are similar (Figure S2 in Supporting Information S1). We note that correlations for South Asian precipitation and PDSI are smaller than those reconstructed for East Asia. This difference likely arises from the sparseness of paleoclimate records from India in both the LMR and PHYDA data sets; in comparison, proxy coverage in East Asia is relatively more robust. Finally, both precipitation and PDSI show large decadal variability over the last 100 years; both data assimilation products capture similar decadal variability, which may be associated with AMO and PDO (Figures 2b and 2d) (Dong & Dai, 2015).

To further validate LMR and PHYDA reconstruction hydroclimate patterns, we compare PDSI from each to a previously published reanalysis soil moisture data set (Dai, 2011) (introduced in Section 2.2). Figure 3 provides

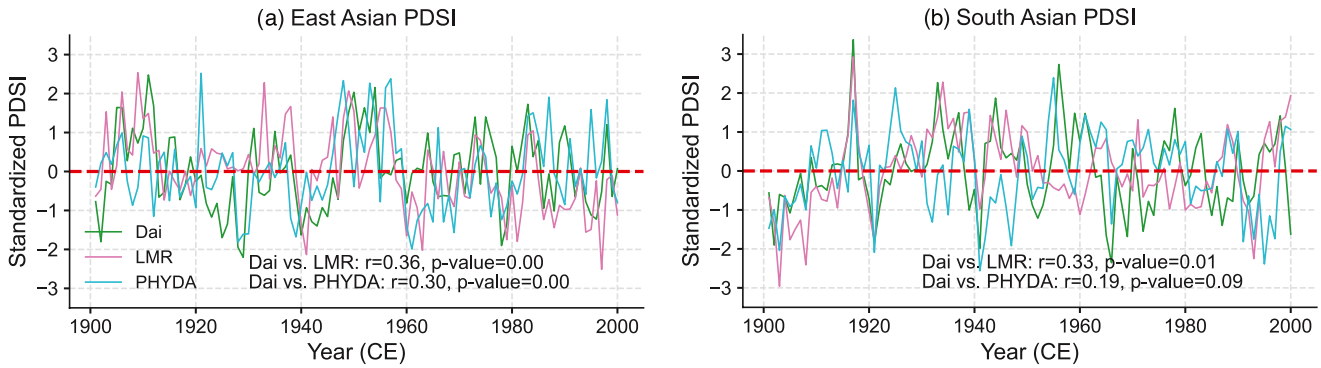

Figure 2. Time series of the East Asian (a) and South Asian (b) Palmer Drought Severity Index (PDSI) from 1900 to 2000, calculated from the Dai PDSI index (green), the Last Millennium Reanalysis (LMR) (magenta), and Paleo-Hydrodynamics Data Assimilation (PHYDA) (blue) data sets. The correlations between the Dai PDSI index and LMR/PHYDA time series together with the corresponding *p* values are annotated at the bottom of each panel. Please note that the Dai PDSI indices are averaged over January-December calendar years.

correlation maps for LMR/PHYDA PDSI and the observation-derived PDSI. Correlations are significant across northern and central China (dotted), but insignificant across much of India and southern China. Overall, the results support the use of the LMR and PHYDA PDSI to study the Asian monsoon, albeit with some spatial heterogeneity in the biases between products in the 20th century.

Since this study focuses on the ENSO-ASM teleconnection, we assess the ability of the LMR and PHYDA to replicate this relationship during the instrumental period. We examined the correlations between the Nino 3.4 index and PDSI using the LMR and observational data (averaged over January-December calendar years, Figure S3 in Supporting Information S1). For PHYDA, observations are averaged over April-March calendar years (Figure S4 in Supporting Information S1). Our results demonstrate that both DA products exhibit significant correlations between Nino 3.4 and PDSI that are comparable to those observed in the 20th century. Specifically, warm SSTs in the Nino 3.4 region correspond to dry conditions in East and South Asia. Furthermore, a comparison of Figures S3b and S4b in Supporting Information S1 suggests that the correlations between ENSO and PDSI averaged over January-December calendar years are consistent with those averaged over April-March calendar years.

3.2. Variation of the ENSO-Monsoon Relationship Over the Last 1,000 Years

We investigate the variation of the relationship between ENSO and ASM by computing the 30-year window moving correlations between East/South Asian PDSI and ENSO indices for LMR and PHYDA (Figure 4).

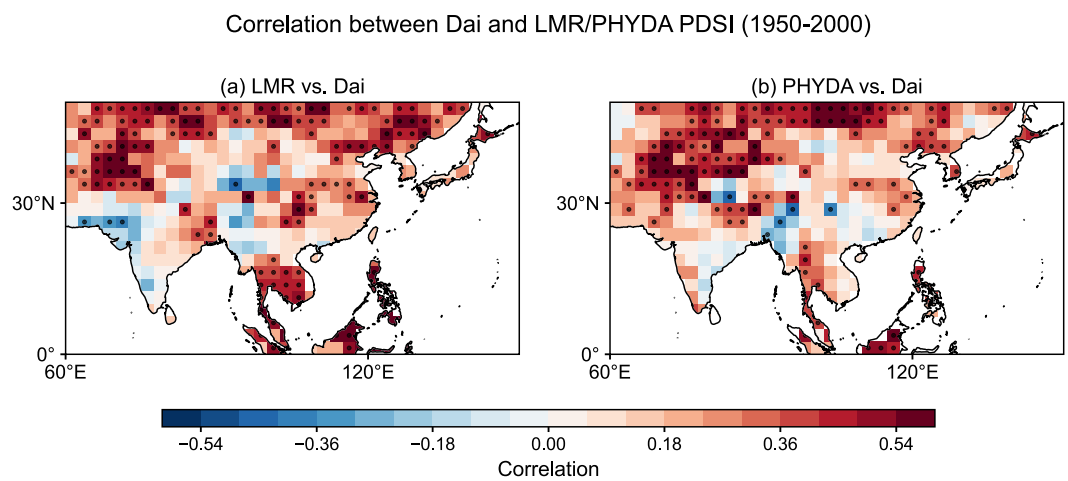

Figure 3. Correlation between the Palmer Drought Severity Index (PDSI) from Dai (2011) and (a) PDSI from the Last Millennium Reanalysis (LMR); (b) PDSI from Paleo-Hydrodynamics Data Assimilation (PHYDA) during 1950–2000 CE. The dotted regions indicate passing the 95% confidence level of the Student's *t*-test.

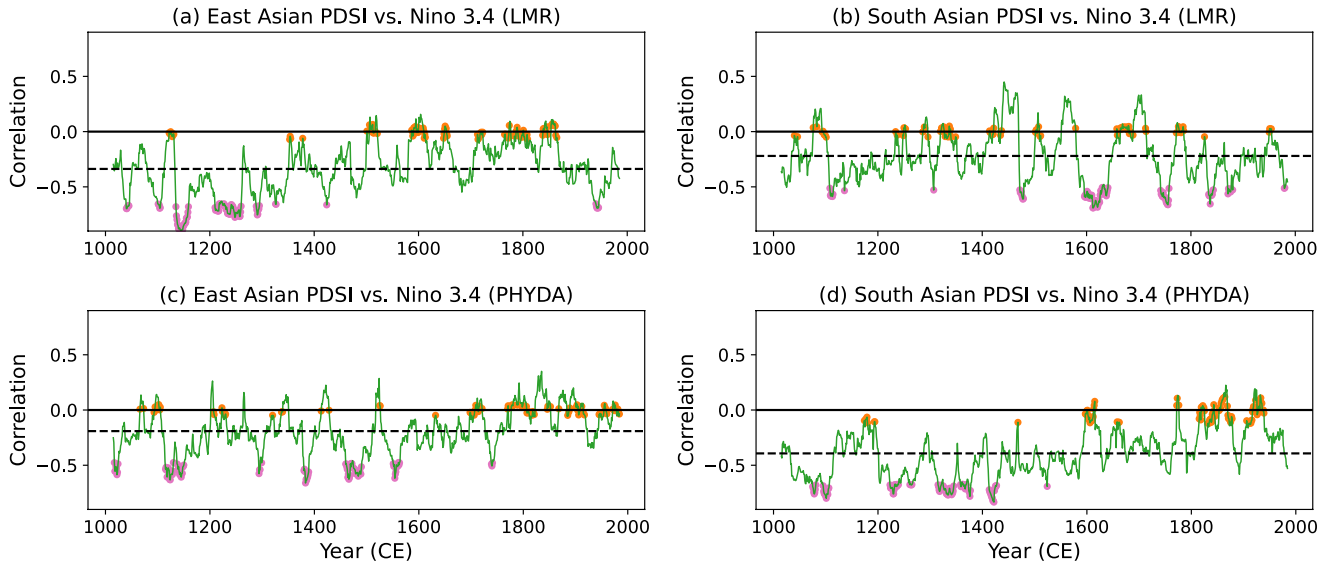

Figure 4. Thirty-year window moving correlation coefficients between El Niño-Southern Oscillation (ENSO) (Nino 3.4 index) and the East Asian monsoon (a, c; Palmer Drought Severity Index (PDSI) index) and the South Asian monsoon (b, d; PDSI index), 1000–2000 CE. The dashed line indicates the mean value of all correlations. Weak ENSO-monsoon teleconnection periods are defined as years when the absolute values of the correlation coefficients (R) are smaller than the tenth percentile of the absolute value of all correlation coefficients (i.e., $0 < |R| <$ tenth percentile ($|R|$)), highlighted in orange). Strong ENSO-monsoon teleconnection periods are defined as years when the correlation coefficient R is less than the tenth percentile of all correlation coefficients ($R <$ tenth percentile (R)), highlighting years when the correlation is strongly negative (highlighted in purple). PDSI and Nino 3.4 index are calculated from (a, b) the Last Millennium Reanalysis (LMR) and (c, d) Paleo-Hydrodynamics Data Assimilation (PHYDA) data sets.

Correlations between ENSO and PDSIs in the monsoon regions are mostly negative (below the solid black lines in Figure 4), but exhibit decadal-to-centennial scale variability. There are also key periods in both LMR (Figures 4a and 4b) and PHYDA (Figures 4c and 4d), and for both the East Asian and South Asian monsoon, where the correlation coefficient is briefly positive, flipping the sign of the teleconnection relationship. The periodicities of the correlation time series are confirmed by spectral analysis. Figure 5 shows that the spectra of the ENSO-EASM and ENSO-SASM correlations have evident peaks around 100–150 years and 30–50 years, the spectra of which exceed an AR1 red noise spectrum at the 95% level.

To relate average SST patterns in the tropical Pacific to the correlation time series shown in Figure 4, we regressed tropical global SST onto both East Asian and South Asian PDSI for the entire last millennium (Figure 6). For the ENSO-EASM teleconnection, the regression maps (Figures 6a and 6c) resemble the SST patterns of La Niña. Negative regression coefficients across the central and eastern tropical Pacific suggest that, when EASM rainfall/PDSI is positive-wet (negative-dry), tropical Pacific SSTs are cool (warm). The regression maps of the ENSO-SASM regression pattern (Figures 6b and 6d) also suggest a link with the PDO (Mantua & Hare, 2002; Newman et al., 2016). Specifically, positive regression coefficients over the northwestern Pacific and negative coefficients over the tropical eastern Pacific suggest that when SASM rainfall/PDSI is positive-wet (negative-dry), the Pacific SST pattern resembles the positive phase of PDO.

3.3. SST and Atmospheric Patterns During Periods of Strong and Weak ENSO-East Asian Summer Monsoon Teleconnection

Figure 4 shows mostly negative correlations between ENSO and the ASM; thus, we next investigate why the ENSO-monsoon correlation is consistently negative during most of the last millennium, but weak or even positive during other periods. Since the correlations are mostly negative over the last millennium, in the following text, the phrase strong ENSO-monsoon teleconnection refers to strong negative correlations between ENSO and monsoon indices. Strong ENSO-monsoon teleconnection periods are defined as years when the correlation coefficient (R) in Figure 4 is less than the tenth percentile of all correlation coefficients ($R <$ tenth percentile (R)), highlighting years when the correlation is strongly negative. Weak ENSO-monsoon teleconnection periods are defined as

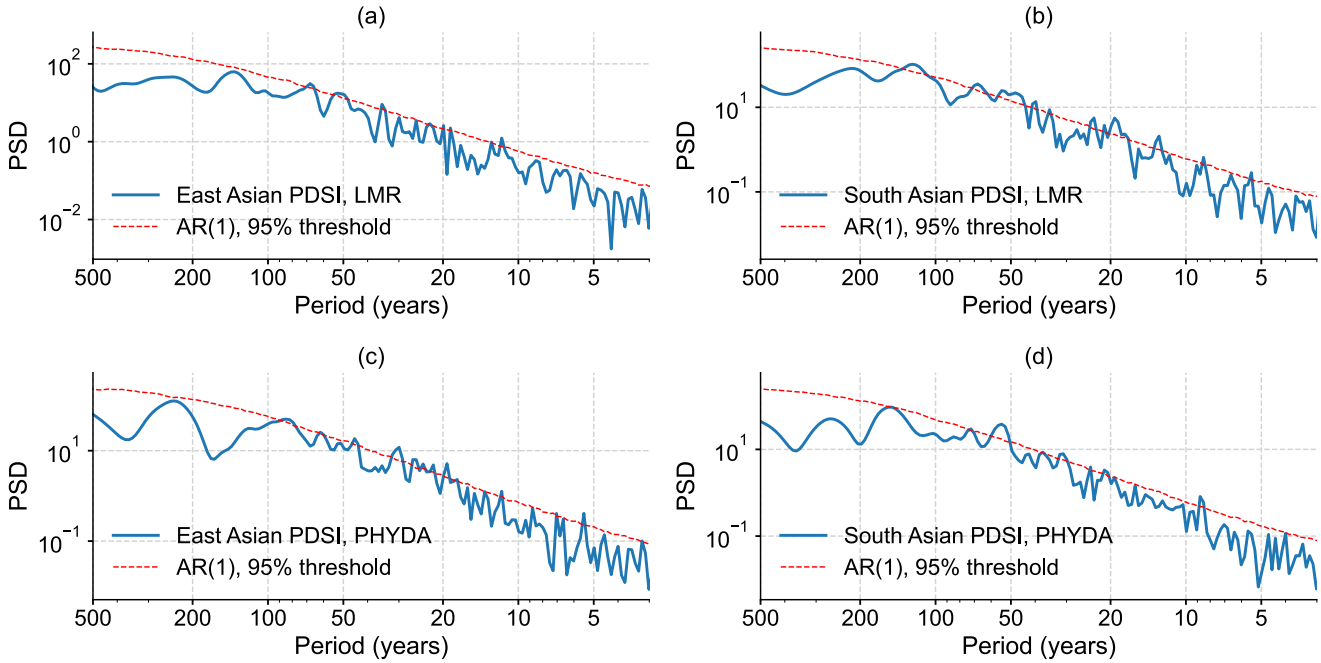

Figure 5. The spectra of the 30-year window moving correlation coefficients between El Niño-Southern Oscillation (ENSO) (Nino 3.4 index) and Palmer Drought Severity Index (PDSI) in the East Asian monsoon region (a, c) and PDSI in the South Asian monsoon region (b, d) indices shown in Figure 4. The PDSI and Nino 3.4 index are calculated from (a, b) the Last Millennium Reanalysis (LMR) and (c, d) Paleo-Hydrodynamics Data Assimilation (PHYDA) data sets. The red dashed lines represent simulated AR(1) benchmark at the 95% level. The calculation and visualization of the spectra are processed using the Python package Pyleoclim (Khider et al., 2022).

years when the absolute values of the correlation coefficients (R) are smaller than the tenth percentile of the absolute value of all correlation coefficients in Figure 4 (i.e., $0 < |R| <$ tenth percentile ($|R|$)). We label these as strong and weak ENSO-monsoon teleconnection periods in purple and orange colors in Figure 4, respectively. Note that the strong (weak) ENSO-monsoon teleconnection periods apply to both phases of ENSO. The duration

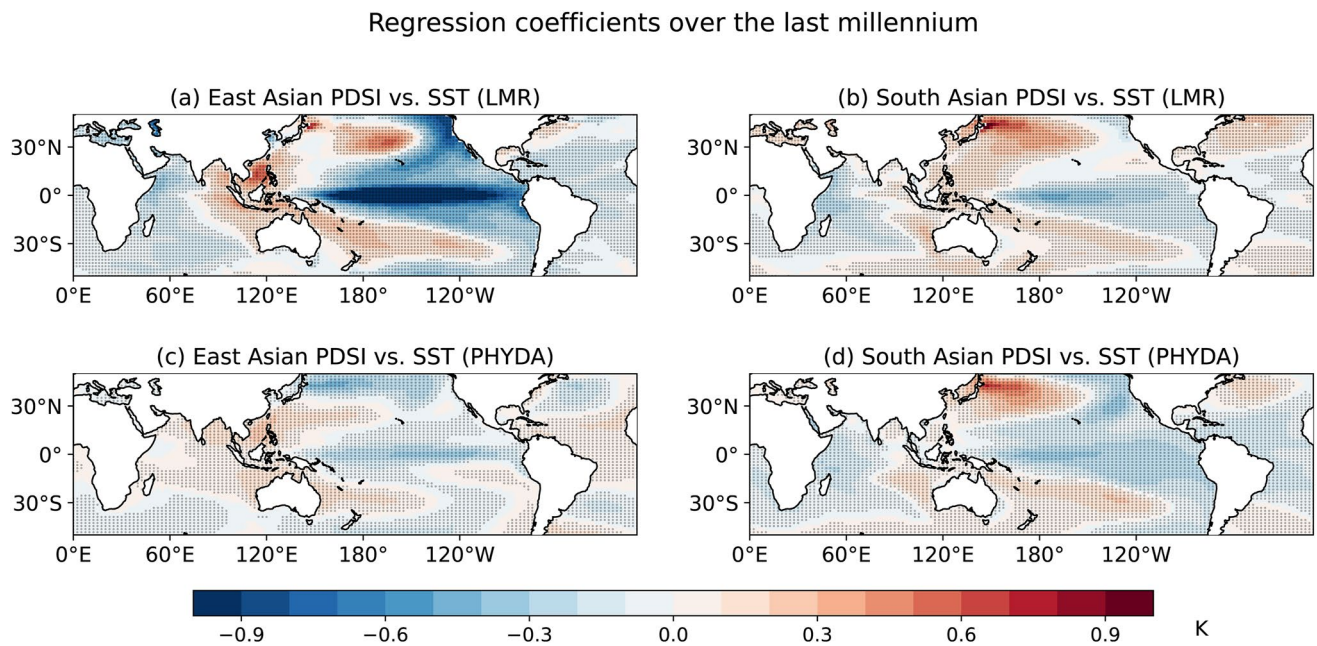

Figure 6. Regression coefficients (unit: K) of sea surface temperature (SST) onto (a, c) East Asian Palmer Drought Severity Index (PDSI) and (b, d) South Asian PDSI over 1000–2000 CE. The PDSI indices are calculated from (a, b) the Last Millennium Reanalysis (LMR) and (c, d) Paleo-Hydrodynamics Data Assimilation (PHYDA) data sets.

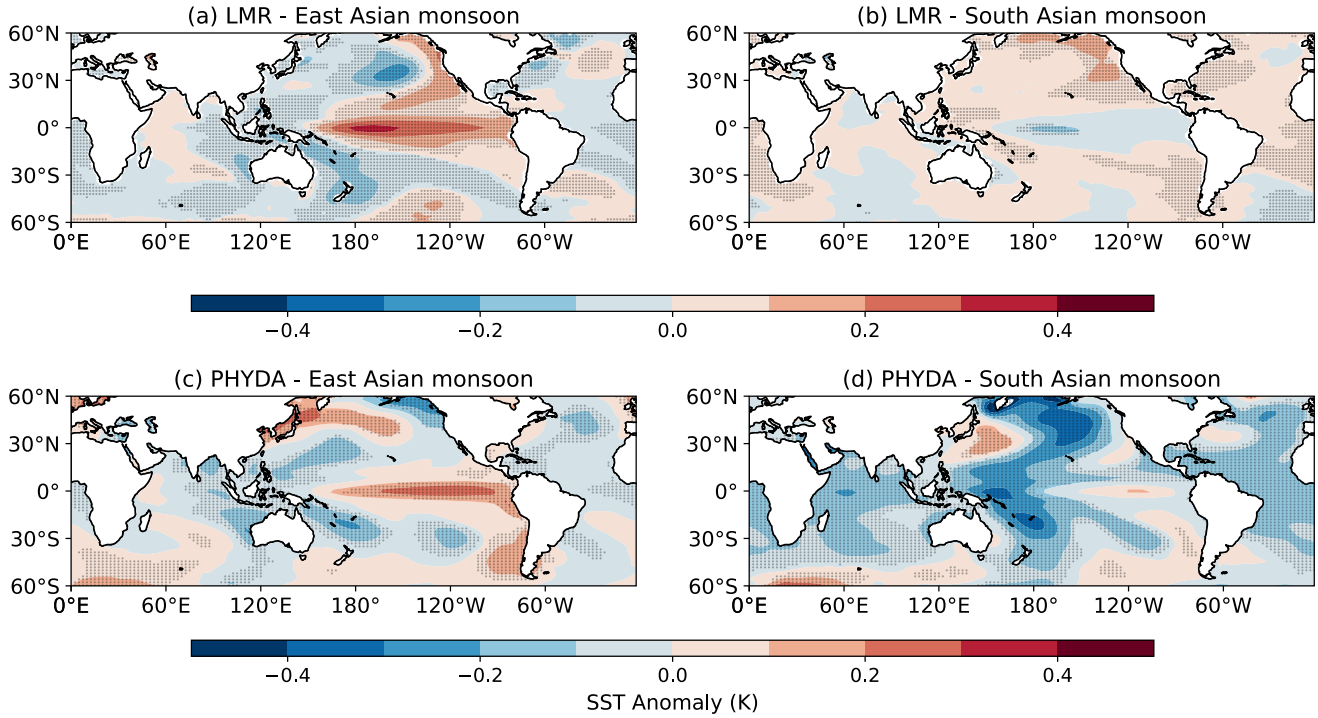

Figure 7. Difference between composites of sea surface temperature (units: K) in periods of weak and strong El Niño-Southern Oscillation-Palmer Drought Severity Index (ENSO-PDSI) correlations. Weak and strong correlation periods are highlighted in orange and purple colors in Figure 4. (a) The sea surface temperature (SST) composites for the ENSO-East Asian PDSI relationship. (b) Shows SST composites for the ENSO-South Asian PDSI relationship. SST and PDSI data are retrieved from (a, b) the Last Millennium Reanalysis (LMR) and (c, d) Paleo-Hydrodynamics Data Assimilation (PHYDA) data sets. Black dots indicate the difference is significant at the 95% confidence level of the Student's *t*-test, considering the impact of autocorrelation on the effective degrees of freedom (Hu et al., 2017).

of these periods is from decades to one century. Using these labeled years, we computed the differences between the weak and strong ENSO-monsoon teleconnection periods for SSTs, geopotential height at 500 hPa, and PDSI to reveal the dynamics governing the ENSO-monsoon teleconnection.

During periods of weak correlations between ENSO and the East Asian summer monsoon, we observe an SST pattern in the Pacific that resembles interannual El Niño events in both LMR and PHYDA (Figures 7a and 7c). This also suggests that, during periods of strong correlations between ENSO and the East Asian summer monsoon, SST patterns are La Niña-like. For the South Asian monsoon, both LMR and PHYDA show warm SST anomalies in the northeastern Pacific, but SST anomalies in PHYDA are not significant (Figures 7b and 7d). In other regions, SST patterns in LMR and PHYDA are not consistent: LMR shows warm SST anomalies across the western Pacific and Indian Ocean, while PHYDA shows cool SST anomalies across the North and South Pacific. This underscores the uncertainties housed in reconstructed PDSI data in the Indian monsoon region due to the lack of paleoclimate proxies included in both LMR and PHYDA from the Indian subcontinent. The inconsistency between LMR and PHYDA might also be due to their different annualization methods. As mentioned in Section 2, the LMR uses a January-December calendar year, while PHYDA uses an April-March calendar year. However, we believe that the primary reason for this inconsistency is the lack of paleoclimate proxies in India. This is in contrast to East Asia, where paleoclimate proxy distribution is relatively denser, potentially yielding a more consistent SST reconstruction between LMR and PHYDA for the EASM.

In addition, we note that while the LMR and PHYDA show similar responses, the magnitudes and locations of warming/cooling centers in these two products are not the same: the center of most intense SST warming during weak ENSO-EASM teleconnection periods is closer to the central tropical Pacific in the LMR compared to PHYDA, and the magnitude of SST cooling over the Pacific during weak ENSO-SASM teleconnection periods is larger in the LMR compared to PHYDA. Considering the similarity of the SST proxy networks in the LMR and PHYDA, the differences between the LMR and PHYDA are likely due to differences in the model priors.

The window sizes chosen for the moving correlations have little effect on our results. We performed similar analyses using window sizes of 20 and 50 years, and the results were comparable (Figures S5 and S6 in Supporting

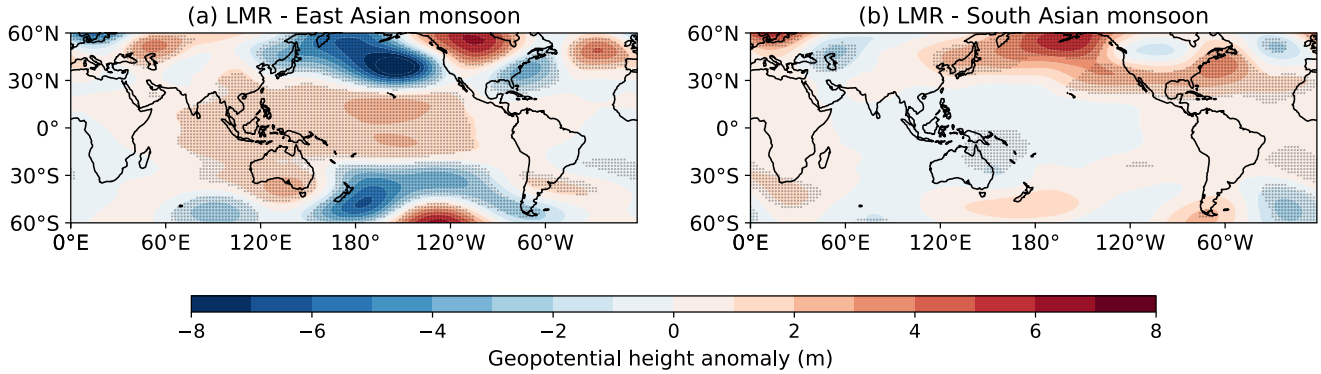

Figure 8. Difference between composites of 500 hPa geopotential height (units: m) in periods of weak and strong El Niño-Southern Oscillation-Palmer Drought Severity Index (ENSO-PDSI) relationship. Weak and strong correlation periods are highlighted in orange and purple colors in Figure 4. (a) The geopotential height composites for the ENSO-East Asian PDSI relationship. (b) The geopotential height composites for the ENSO-South Asian PDSI relationship. SST and PDSI data are retrieved from the Last Millennium Reanalysis (LMR) data sets. Black dots indicate the difference is significant at the 95% confidence level of the Student's *t* test.

Information S1). To determine the impact of decadal variability on our findings, we applied a 2–9 years band-pass filter to the SST and PDSI fields. The resulting moving correlation time series was largely comparable to our original results (Figure S7 in Supporting Information S1); the correlation between the correlation time series in Figure S7 in Supporting Information S1 and Figure 4 ranged between 0.7 and 0.8, surpassing the 95% level of the Student's *t* test, considering the impact of autocorrelation on the effective degrees of freedom (Hu et al., 2017).

To confirm that the similarity in SST patterns exhibited in the LMR and PHYDA shown in Figure 7a (a) is not due to their shared model prior, and (b) that the prior does not have an outsized influence on the ENSO-ASM teleconnection results analyzed here, we conducted a comparative analysis of the SST composite differences using an ensemble member of the CESM-LME data (Figure S8 in Supporting Information S1). The results obtained using the model prior, CESM-LME, are markedly different from those of the LMR and PHYDA. Specifically, for the East Asian monsoon, the largest SST response occurs in the northeastern Pacific instead of the central Pacific. For the South Asian monsoon, the largest SST response occurs over the Warm Pool region and the northwestern Pacific, rather than the North Pacific and Atlantic. Therefore, we assert that the ENSO-monsoon teleconnection signals observed in the LMR and PHYDA mainly originate from information derived from the paleoclimate proxies, rather than their model priors.

Geopotential height patterns for weak minus strong correlation periods (Figure 8) indicate that periods of weak correlation between ENSO and the East Asian summer monsoon are associated with an atmospheric circulation pattern typical during canonical El Niño events: anomalously high geopotential height over the tropical Pacific and anomalously low geopotential height over the midlatitude Pacific (Figure 8a). In contrast, during weak correlations for the SASM, anomalously high geopotential height is observed north of 30°N (Figure 8b), which explains the warm SST anomalies in the northeastern Pacific in Figure 7d.

Finally, we examined PDSI patterns during the periods of weak versus strong correlations between ENSO and the East and South Asian summer monsoons. The PDSI patterns are consistent in both LMR and PHYDA for the ENSO-EASM relationship. Specifically, both products reconstruct decreased precipitation in East China and increased precipitation in central Asia (Figures 9a and 9c) during periods of weak ENSO-EASM teleconnections. However, the PDSI patterns for weak ENSO-SASM correlation periods are not consistent between LMR and PHYDA (Figures 9b and 9d). LMR shows decreased precipitation in India but PHYDA shows the opposite.

To zoom in on the differences in ENSO teleconnection-related precipitation for weak versus strong ENSO-EASM and ENSO-SASM teleconnection periods, we calculated the composite differences (weak minus strong teleconnection periods) for PDSI comparing El Niño and La Niña years (Figure 10). El Niño (La Niña) years in both weak and strong teleconnection periods are selected if the Nino 3.4 index is above (below) one standard deviation of the Nino 3.4 index in the last 1,000 years Figure 10 shows the difference in PDSI between El Niño and La Niña years during weak and strong teleconnection periods. We find that during strong ENSO-EASM teleconnection periods, PDSI is more negative (brown color) in El Niño years when compared to La Niña years in East Asia (Figures 10b and 10d). In contrast, during weak ENSO-EASM teleconnection periods, PDSI is more

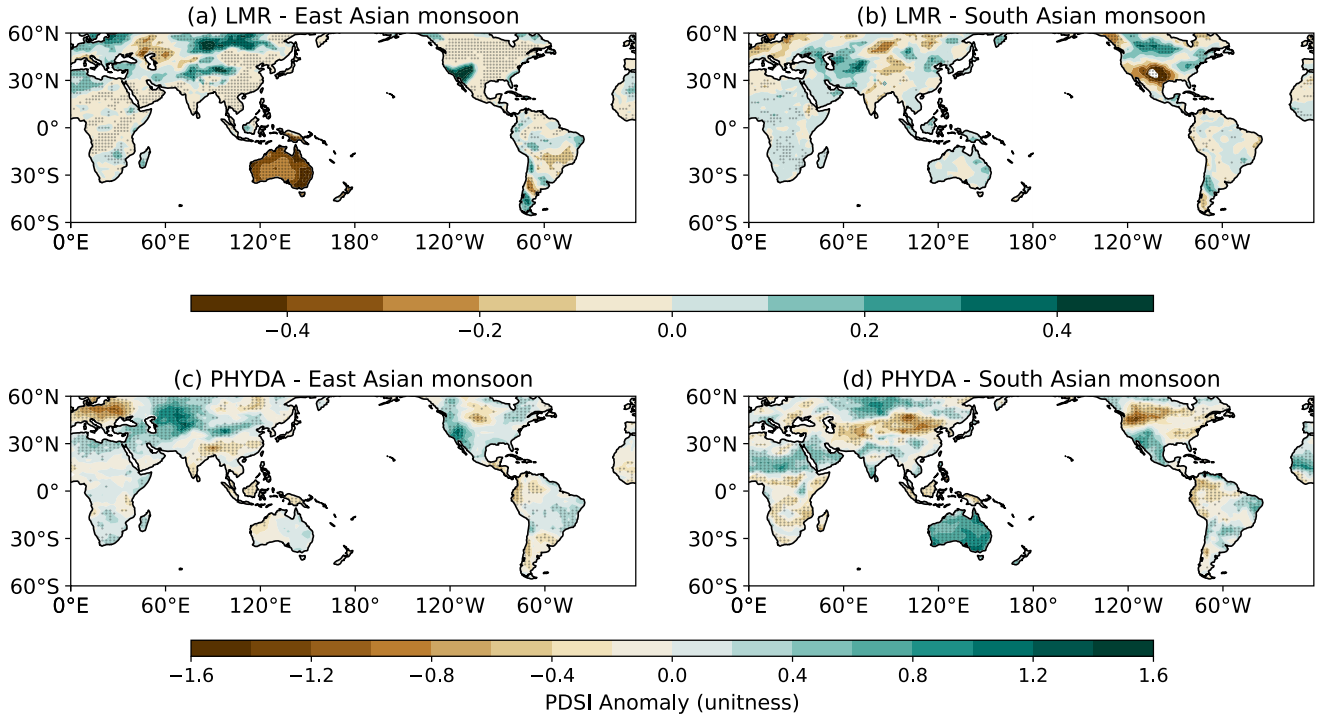

Figure 9. Difference between composites of PDSI in periods of weak and strong El Niño-Southern Oscillation-Palmer Drought Severity Index (ENSO-PDSI) relationship. Weak and strong correlation periods are highlighted in orange and purple colors in Figure 4. (a) PDSI composites for the ENSO-East Asian PDSI relationship. (b) PDSI composites for the ENSO-South Asian PDSI relationship. PDSI data are retrieved from (a, b) the Last Millennium Reanalysis (LMR) and (c, d) Paleo-Hydrodynamics Data Assimilation (PHYDA) data sets. Black dots indicate the difference is significant at the 95% confidence level of the Student's *t* test.

positive (wetter conditions) during El Niño years compared to La Niña years in the Yangtze River Valley region (Figures 10a and 10c). We also note PHYDA data shows that PDSI is more positive in the Philippines during strong ENSO-EASM teleconnection periods, while it is more negative in weak ENSO-EASM teleconnection periods, but this opposite response is not shown in the LMR data. A similar analysis for the South Asian monsoon shows that PDSI is more negative in El Niño years compared to La Niña years during strong ENSO-SASM teleconnection periods in South Asia (Figures 11b and 11d). During weak ENSO-SASM teleconnection periods, there is increased PDSI during El Niño years compared to La Niña years in northeast India (Figures 11a and 11c). These results are consistent in both LMR and PHYDA. We note that there are large differences between the LMR and PHYDA in the composite difference maps during weak ENSO-SASM teleconnection periods (Figures 11a and 11c). The large differences in eastern China are likely due to the sparseness of proxy records in both LMR and PHYDA in this region, causing the reconstructions to rely more heavily on their different GCM priors.

4. Discussion and Conclusions

The East and South Asian Summer Monsoon systems modulate water supply to billions of people, and are highly variable. Part of this variability is driven by ENSO, which can enhance or dampen Asian monsoon rainfall. To better characterize the behavior of the ASM and extend the 20th century record, this study examined the evolution of the ENSO-ASM teleconnection over the last 1,000 years using two paleoclimate data assimilation reconstructions, LMR and PHYDA. The reconstruction of the ASM was validated in both products using observationally-derived PDSI, and while biases indeed exist, the agreement between both LMR and PHYDA and observations of the EASM and SASM over the 20th century is significant (Figures 1–3). Overall, validation statistics show the LMR/PHYDA reconstructed PDSI is more reliable in northern and central China than in southeast China and northern India. In addition, the LMR correlates with PDSI data sets better than PHYDA in East Asia.

A regression analysis relating SSTs to the ASM over the last 1,000 years suggests that tropical Pacific SSTs exert an influence on the EASM such that cooler La Niña-like surface-ocean patterns enhance rainfall, whereas warmer

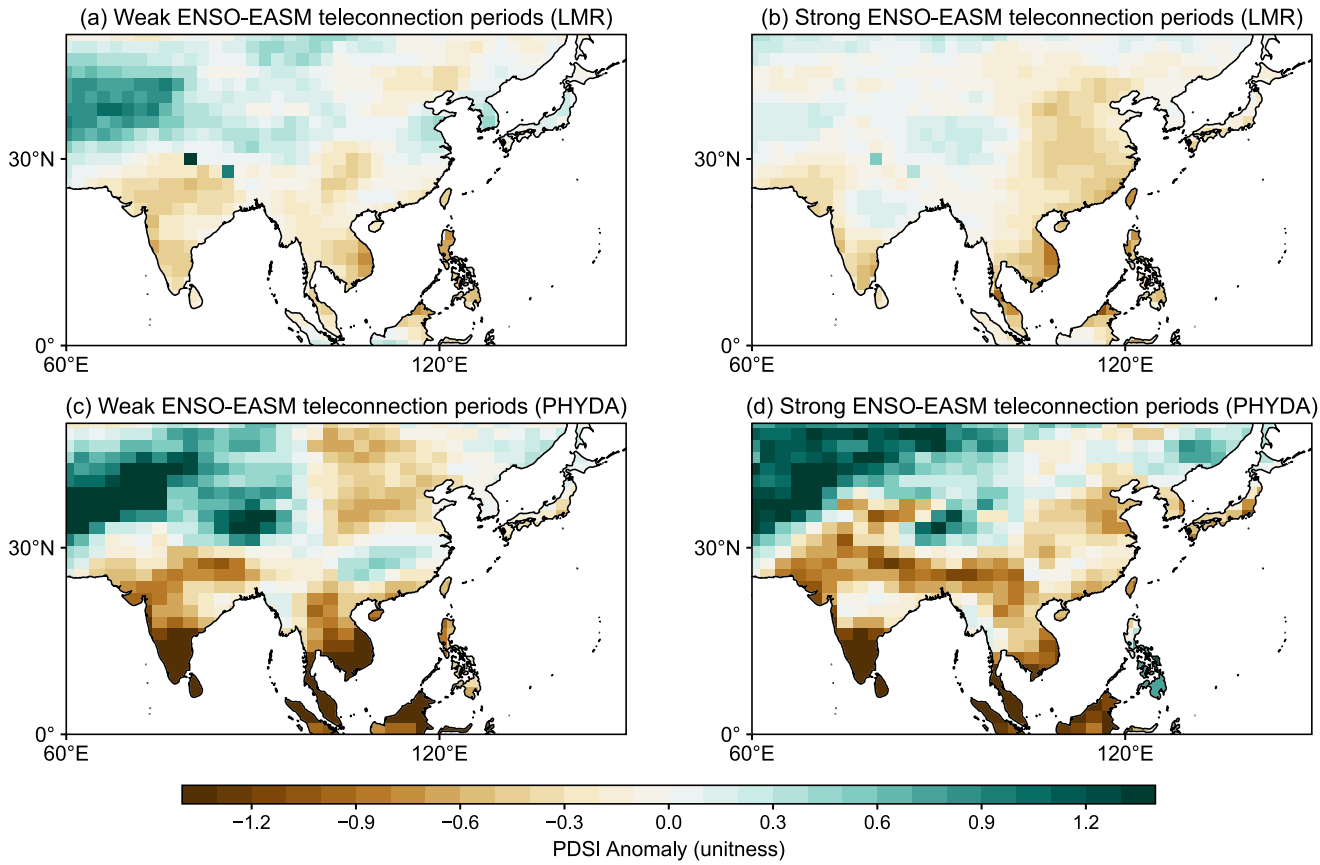

Figure 10. Composite difference of Asian Palmer Drought Severity Index (PDSI) (unit = 1) between El Niño years and La Niña years during weak (a, c) and strong (b, d) El Niño-Southern Oscillation (ENSO)-East Asian summer monsoon teleconnection periods highlighted in Figure 4. The PDSI data are retrieved from the Last Millennium Reanalysis (LMR) (a, b) and Paleo-Hydrodynamics Data Assimilation (PHYDA) (c, d).

SSTs in the central Pacific suppress rainfall (Figures 6a and 6c). By contrast, the SASM regression reveals a pattern resembling the canonical PDO pattern (Figures 6b and 6d), suggesting sensitivity to decadal processes in the Pacific Ocean; a positive (negative) phase of the PDO leads to wetter (drier) SASM (Section 3.2) (Midhun et al., 2022).

Previous work has focused on the significance and variability of the ENSO-ASM relationship over the 20th century (Kumar et al., 2006; Kumar, Kleeman, et al., 1999; Torrence & Webster, 1999; Wang, 2002; Wu & Wang, 2002). Our work suggests that the strength of the ENSO-ASM teleconnection in the 20th century is not unique. There are other periods of time with significant ENSO-monsoon correlations (e.g., 1000–1100 CE, 1300–1400 CE for the East Asian monsoon and 1000–1100 CE, 1300–1400 CE for the South Asian monsoon) (Figure 4). Indeed, the ENSO-ASM relationship is nonstationary (Figure 4), and ranges widely between periods exhibiting significant positive correlations, no correlation, and significant negative correlations; the relationship also exhibits robust decadal-centennial variability (Figure 5). However, our analysis suggests that *on average* over the last millennium, there is a negative correlation between the NINO3.4 index (central Pacific SSTs) and both EA and SA monsoon rainfall intensity (Section 3.2).

To evaluate the dynamics controlling the strength of the ENSO-ASM teleconnection, we additionally produced composite SST and geopotential height fields for periods of weak and strong ENSO-ASM correlations (as highlighted in Figures 7–9, Section 3.3). Broadly, when the teleconnection between ENSO and the East Asian summer monsoon is weak (strong), SSTs in the eastern Pacific are warmer (cooler) than normal, though we note that the SST warming center in the tropical Pacific based on the LMR is closer to the central Pacific, while the warming center from PHYDA is closer to the eastern Pacific. When the teleconnection between ENSO and the South Asian summer monsoon is weak, SST patterns are not consistent between the LMR and PHYDA. Uncertainties housed in reconstructed PDSI data in the Indian monsoon region are likely driven by a lack of

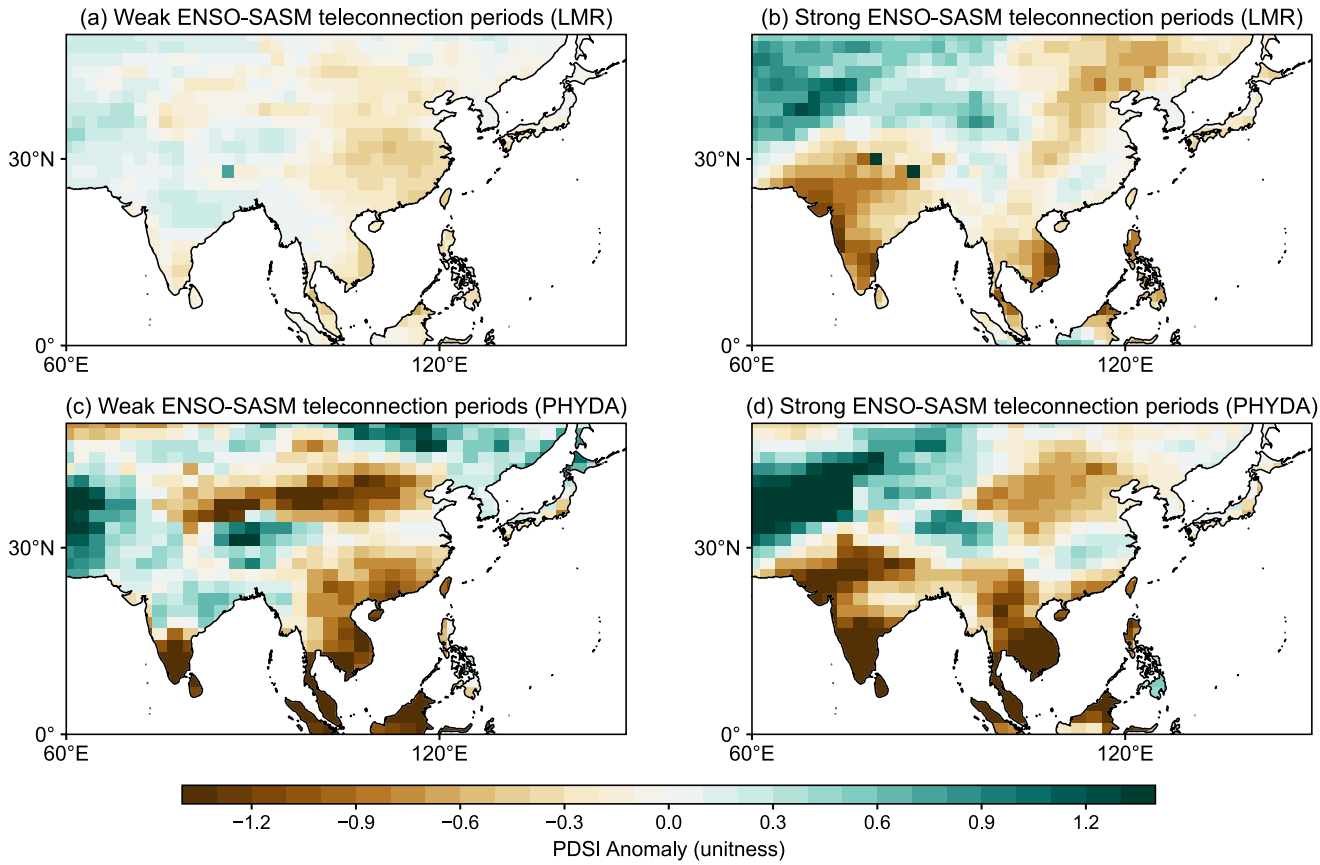

Figure 11. Composite difference of Asian Palmer Drought Severity Index (PDSI) (unit = 1) between El Niño years and La Niña years during weak (a, c) and strong (b, d) El Niño-Southern Oscillation (ENSO)-South Asian summer monsoon teleconnection periods highlighted in Figure 4. The PDSI data are retrieved from the Last Millennium Reanalysis (LMR) (a, b) and Paleo-Hydrodynamics Data Assimilation (PHYDA) (c, d).

paleoclimate proxies included in both LMR and PHYDA from the Indian subcontinent. Critically, a great many more hydroclimate proxies from this region are needed to improve data assimilation reconstruction skill, and to better study the interannual-interdecadal variability of the SASM. In addition, the composite differences of Asian PDSI between El Niño and La Niña years (Figures 10 and 11) indicate that the Yangtze River Valley and northeastern India are critical regions where the variation of the ENSO-ASM teleconnection exerts a strong influence on seasonal rainfall. When the ENSO-ASM teleconnection is weak, the Yangtze River Valley and northeastern India are wet instead of dry during strong ENSO-ASM teleconnection periods.

Data spanning the 20th century are consistent: when strong El Niño events occur, boreal summer monsoon rainfall over Asia decreases. Our analyses extend this conclusion to decadal-centennial scales over the last millennium and suggest cool (warm) tropical Pacific conditions typically dominate during wet (dry) monsoon years. There are notable exceptions, as highlighted in (Nanjundiah et al., 2013): the 97–98 event, one of the strongest Eastern Pacific El Niño events on record, occurred alongside a strong summer monsoon. Understanding these "outlier" events is crucial for the prediction of the ASM; paleoclimate archives documenting such events may lend insight into why the relationship occasionally flips signs. Figure 4 suggests there are periods over the last 1,000 years where the ENSO-ASM correlation is positive (e.g., a strong monsoon occurs alongside El Niño-like conditions). During periods where the ENSO-EASM correlation is positive, SSTs in the central-eastern Pacific are warmer than normal, and eastern Indian Ocean SSTs are cooler (resembling a positive phase of the IOD) (Figure 7). This is consistent with previous studies, suggesting that the Indian Ocean acts as an "capacitor," storing the El Niño signal by changing the SST pattern to a positive phase of IOD through weakening the Walker Circulation in spring and summer, extending and strengthening the influence of ENSO in winter (Zhang et al., 2022).

We acknowledge important limitations of this work. First, the paleoclimate data assimilation products used here lack critical dynamical fields, specifically winds. We are limited to temperature and hydroclimate patterns,

though the LMR does reconstruct geopotential height. Extension work evaluating model simulations spanning the last 1,000 years is underway in companion work, and will enhance our analysis of the dynamics underlying the ENSO-ASM teleconnection. Both the LMR and PHYDA contain important uncertainties. Uncertainties stem from measurement errors, age uncertainties, interpretations of proxy data, and the model prior. The products suffer from variance loss during the earlier parts of the reconstructions as a function of proxy availability (Steiger et al., 2018). In particular, the DA reconstruction in the areas without sufficient coverage of proxy records is likely largely dependent on the model prior. Revisiting the proxy coverage of both LMR and PHYDA, we note that PDSI data in India may have larger uncertainties than in other Asian monsoon areas due to the sparse proxy coverage. As mentioned above, this underscores the importance of developing more paleoclimate proxies in the Indian subcontinent. As shown in Figures 1 and 2, correlations between precipitation and PDSI in PHYDA and LMR and instrumental observations over the ASM regions are approximately 0.3–0.4; while these correlations are statistically significant, they capture only a small fraction of the variations in instrumental records. While the LMR and PHYDA arguably are the "state-of-the-art" in terms of available data products we can use to look at the long-term variations of the ENSO-ASM teleconnection, their reliability is inherently limited by proxy availability. Enhancing the proxy network used in the DA reconstructions with historical written documents is one option for bolstering existing reconstructions (Hao et al., 2016; Zhang, 1991); such improvements are underway amongst the authors of this work.

In general, all paleoclimate data assimilation products are dependent on the climate patterns of their model prior, and these climate models contain biases (Amrhein et al., 2020; Parsons & Hakim, 2019) which impact the spatial patterns of SST and PDSI evaluated here. For example, the CESM-LME forms the climate model prior for PHYDA, and thus the hydroclimate and SST patterns reconstructed in PHYDA are necessarily based on the air-sea relationships in CESM, a model known to have an amplified representation of ENSO and its teleconnection (Deser et al., 2012). Model grid scale and spatial resolution may also limit the accurate simulation of hydrological cycle variables such as precipitation and PDSI (Kumar et al., 2022; Muetzelfeldt et al., 2021). PHYDA uses a bias-correction technique to nudge the reconstruction toward observations, however (Steiger et al., 2019), partially resolving these issues.

We note that there are nontrivial differences between the results based on the LMR and PHYDA, including the precipitation time series (Figure 1), the moving correlation time series (Figure 4) and the teleconnection patterns (Figures 7–9). The differences are likely due to the differences in proxy networks and the model prior (as discussed in Section 2a). PHYDA used the CESM Last Millennium Ensemble simulations (Otto-Bliesner et al., 2016), while the LMR used the CMIP5 Last Millennium simulation of CCSM4 (Landrum et al., 2013). Furthermore, the CESM-LME used in PHYDA was bias-corrected to observations, whereas the LMR framework applied no bias-correction (Steiger et al., 2018). In addition, the LMR and PHYDA used different approaches to generate their respective model priors. The model prior used in the LMR is the same in all years over the last millennium; PHYDA used the transient evolution of climate states, so the LMR does not contain time-specific information about climate events. Despite the differences between the LMR and PHYDA, the fact that these two products exhibit similar spatial patterns bolsters our conclusions and lends confidence toward the fact that the proxy signals are strong and coherent between different products in the ASM region.

In summary, we investigated the variation of the ENSO-ASM teleconnections in the last 1,000 years with data assimilation products. We first demonstrated the quality of two data assimilation products, LMR and PHYDA, which are both sufficient in terms of their reconstructions of SST and PDSI for studying the Asian monsoon over the last 1,000 years. We posed three key questions in Section 1: *(a) How does the ENSO-ASM relationship change over the last millennium? (b) Do historically observed ENSO-monsoon teleconnection relationships hold in the past? and (c) What are the dynamics associated with periods of strong and weak ENSO-ASM teleconnections?* Our results show that (a) the ENSO teleconnections to the Asian summer monsoon have evident decadal-to-centennial scale variability, but with strong asymmetry in the last 1,000 years. During most of the last 1,000 years, El Niño tends to be associated with weak ASMs. (b) Consistent with previous studies based on instrumental data, variation of the ENSO-ASM teleconnections is related to SST pattern changes. (c) Weak ENSO-East Asian summer monsoon teleconnection is associated with SST anomalies resembling El Niño events.

In closing, climate model ensemble simulations suggest large changes to the global hydrological cycle. Hydroclimate extremes driven by the ASM are no exception and may change in a warming climate (Rajesh & Goswami, 2022; Saranya et al., 2022; Sarkar & Maity, 2022). Both strong and weak monsoons have the potential

to critically disrupt agriculture, damage infrastructure via flooding, and impact water supply (Wang et al., 2022). Generating a more robust understanding of future hydroclimate extremes in the ASM region depends on accurate statistics surrounding the role of natural variability in modulating rainfall. To this end, paleoclimate reconstructions yield thousands of years of SST and PDSI patterns at annual resolution and can provide long-term constraints on the ENSO-ASM relationship and the climatic controls on ASM strength. A robust understanding of the ENSO-ASM relationship is sorely needed for risk assessment and regional adaptation strategies in a changing climate. This work is a first step in documenting how modes of tropical Pacific variability will modulate the ASM, a signal which will compound with climate change; we hope this and future work may advance our knowledge of future climate risks in Asia.

Conflict of Interest

The authors declare no conflicts of interest relevant to this study.

Data Availability Statement

The LMR data can be accessed via https://doi.org/10.25921/gn22-5866 (Tardif et al., 2019b). The PHYDA data are available via https://doi.org/10.5281/zenodo.1198817 (Steiger, 2018). The GPCC data are available via https://doi.org/10.5676/DWD_GPCC/FD_M_V7_250 (Schneider et al., 2015). The Dai PDSI data can be accessed via https://doi.org/10.5065/D6QF8R93 (Dai, 2017).

Acknowledgments

This work was supported by the National Science Foundation Paleoclimate Perspectives on Climate Change (P2C2) Award 2102814 to J.H. and S.D. and 2102812 to K.T. We appreciate Feng Zhu and Nathan Steiger's assistance with accurate use and interpretation of LMR and PHYDA. We appreciate constructive comments from Dr. Mukund Palat Rao and two anonymous reviewers, which greatly improved this work.

References

Abram, N. J., Gagan, M. K., Liu, Z., Hantoro, W. S., McCulloch, M. T., & Suwargadi, B. W. (2007). Seasonal characteristics of the Indian Ocean Dipole during the Holocene epoch. *Nature*, *445*(7125), 299–302. https://doi.org/10.1038/nature05477

Almazroui, M., Saeed, F., Saeed, S., Ismail, M., Ehsan, M. A., Islam, M. N., et al. (2021). Projected changes in climate extremes using CMIP6 simulations over SREX regions. *Earth Systems and Environment*, *5*(3), 481–497. https://doi.org/10.1007/s41748-021-00250-5

Amrhein, D. E., Hakim, G. J., & Parsons, L. A. (2020). Quantifying structural uncertainty in paleoclimate data assimilation with an application to the last millennium. *Geophysical Research Letters*, *47*, e2020GL090485. https://doi.org/10.1029/2020GL090485

Anderson, D., Tardif, R., Horlick, K., Erb, M., Hakim, G., Noone, D., et al. (2019). Additions to the last millennium reanalysis multi-proxy database. *Data Science Journal*, *18*(1), 2. https://doi.org/10.5334/dsj-2019-002

Ashok, K., Guan, Z., & Yamagata, T. (2001). Impact of the Indian Ocean dipole on the relationship between the Indian monsoon rainfall and ENSO. *Geophysical Research Letters*, *28*(23), 4499–4502. https://doi.org/10.1029/2001GL013294

Ashrit, R., Kumar, K. R., & Kumar, K. K. (2001). ENSO-monsoon relationships in a greenhouse warming scenario. *Geophysical Research Letters*, *28*(9), 1727–1730. https://doi.org/10.1029/2000GL012489

Becker, A., Finger, P., Meyer-Christoffer, A., Rudolf, B., Schamm, K., Schneider, U., & Ziese, M. (2013). A description of the global land-surface precipitation data products of the global precipitation climatology centre with sample applications including centennial (trend) analysis from 1901-present. *Earth System Science Data*, *5*(1), 71–99. https://doi.org/10.5194/essd-5-71-2013

Berkelhammer, M., Sinha, A., Mudelsee, M., Cheng, H., Yoshimura, K., & Biswas, J. (2014). On the low-frequency component of the ENSO-Indian monsoon relationship: A paired proxy perspective. *Climate of the Past*, *10*(2), 733–744. https://doi.org/10.5194/cp-10-733-2014

Breitenmoser, P., Brönnimann, S., & Frank, D. (2014). Forward modelling of tree-ring width and comparison with a global network of tree-ring chronologies. *Climate of the Past*, *10*(2), 437–449. https://doi.org/10.5194/cp-10-437-2014

Cash, B. A., Barimalala, R., Kinter, J. L., Altshuler, E. L., Fennessy, M. J., Manganello, J. V., et al. (2017). Sampling variability and the changing ENSO–monsoon relationship. *Climate Dynamics*, *48*(11), 4071–4079. https://doi.org/10.1007/s00382-016-3320-3

Chan, J. C., & Zhou, W. (2005). PDO, ENSO and the early summer monsoon rainfall over south China. *Geophysical Research Letters*, *32*, L08810. https://doi.org/10.1029/2004GL022015

Cherchi, A., Terray, P., Ratna, S. B., Sankar, S., Sooraj, K. P., & Behera, S. (2021). Chapter 8—Indian Ocean Dipole influence on Indian summer monsoon and ENSO: A review. In J. Chowdary, A. Parekh, & C. Gnanaseelan (Eds.), *Indian summer monsoon variability* (pp. 157–182). Elsevier. https://doi.org/10.1016/B978-0-12-822402-1.00011-9

Dai, A. (2011). Characteristics and trends in various forms of the palmer drought severity index during 1900–2008. *Journal of Geophysical Research*, *116*, D12115. https://doi.org/10.1029/2010JD015541

Dai, A. (2017). Dai global palmer drought severity index (PDSI) [Dataset]. Research Data Archive at the National Center for Atmospheric Research. https://doi.org/10.5065/D6QF8R93

Dai, A., & Wigley, T. M. L. (2000). Global patterns of ENSO-induced precipitation. *Geophysical Research Letters*, *27*(9), 1283–1286. https://doi.org/10.1029/1999GL011140

Dee, S. G., Steiger, N. J., Emile-Geay, J., & Hakim, G. J. (2016). On the utility of proxy system models for estimating climate states over the Common era. *Journal of Advances in Modeling Earth Systems*, *8*, 1164–1179. https://doi.org/10.1002/2016MS000677

Deser, C., Phillips, A. S., Tomas, R. A., Okumura, Y. M., Alexander, M. A., Capotondi, A., et al. (2012). ENSO and pacific decadal variability in the Community climate system model version 4. *Journal of Climate*, *25*(8), 2622–2651. https://doi.org/10.1175/JCLI-D-11-00301.1

Dong, B., & Dai, A. (2015). The influence of the interdecadal pacific oscillation on temperature and precipitation over the globe. *Climate Dynamics*, *45*(9), 2667–2681. https://doi.org/10.1007/s00382-015-2500-x

Dong, B., Dai, A., Vuille, M., & Timm, O. E. (2018). Asymmetric modulation of ENSO teleconnections by the interdecadal pacific oscillation. *Journal of Climate*, *31*(18), 7337–7361. https://doi.org/10.1175/JCLI-D-17-0663.1

Du, Y., Xie, S.-P., Huang, G., & Hu, K. (2009). Role of air-sea interaction in the long persistence of El Niño–induced north Indian Ocean warming. *Journal of Climate*, *22*(8), 2023–2038. https://doi.org/10.1175/2008JCLI2590.1

Emile-Geay, J., McKay, N. P., Kaufman, D. S., von Gunten, L., Wang, J., Anchukaitis, K. J., et al. (2017). A global multiproxy database for temperature reconstructions of the Common Era. *Scientific Data*, *4*(1), 170088. https://doi.org/10.1038/sdata.2017.88

Eroglu, D., McRobie, F. H., Ozken, I., Stemler, T., Wyrwoll, K.-H., Breitenbach, S. F., et al. (2016). See-saw relationship of the Holocene East Asian-Australian summer monsoon. *Nature Communications*, *7*(1), 1–7. https://doi.org/10.1038/ncomms12929

Gadgil, S., & Kumar, K. R. (2006). The Asian monsoon—Agriculture and economy. In *The Asian monsoon* (pp. 651–683). Springer.

Gershunov, A., Schneider, N., & Barnett, T. (2001). Low-frequency modulation of the ENSO-Indian monsoon rainfall relationship: Signal or noise? *Journal of Climate*, *14*(11), 2486–2492. https://doi.org/10.1175/1520-0442(2001)014<2486:LFMOTE>2.0.CO;2

Goswami, B., Madhusoodanan, M., Neema, C., & Sengupta, D. (2006). A physical mechanism for North Atlantic SST influence on the Indian summer monsoon. *Geophysical Research Letters*, *33*, L02706. https://doi.org/10.1029/2005GL024803

Ha, K., Moon, S., Timmermann, A., & Kim, D. (2020). Future changes of summer monsoon characteristics and evaporative demand over Asia in CMIP6 simulations. *Geophysical Research Letters*, *47*, e2020GL087492. https://doi.org/10.1029/2020GL087492

Hakim, G. J., Emile-Geay, J., Steig, E. J., Noone, D., Anderson, D. M., Tardif, R., et al. (2016). The last millennium climate reanalysis project: Framework and first results. *Journal of Geophysical Research: Atmospheres*, *121*, 6745–6764. https://doi.org/10.1002/2016JD024751

Hao, Z., Zheng, J., Zhang, X., Liu, H., Li, M., & Ge, Q. (2016). Spatial patterns of precipitation anomalies in eastern China during centennial cold and warm periods of the past 2000 years. *International Journal of Climatology*, *36*(1), 467–475. https://doi.org/10.1002/joc.4367

Hong, L.-C., LinHo, & Jin, F.-F. (2014). A southern hemisphere booster of super El Niño. *Geophysical Research Letters*, *41*, 2142–2149. https://doi.org/10.1002/2014GL059370

Hu, J., Emile-Geay, J., & Partin, J. (2017). Correlation-based interpretations of paleoclimate data—Where statistics meet past climates. *Earth and Planetary Science Letters*, *459*, 362–371. https://doi.org/10.1016/j.epsl.2016.11.048

Katzenberger, A., Schewe, J., Pongratz, J., & Levermann, A. (2021). Robust increase of Indian monsoon rainfall and its variability under future warming in CMIP6 models. *Earth System Dynamics*, *12*(2), 367–386. https://doi.org/10.5194/esd-12-367-2021

Khider, D., Emile-Geay, J., Zhu, F., James, A., Landers, J., Ratnakar, V., & Gil, Y. (2022). Pyleoclim: Paleoclimate timeseries analysis and visualization with python. *Paleoceanography and Paleoclimatology*, *37*, e2022PA004509. https://doi.org/10.1029/2022PA004509

Khodri, M., Izumo, T., Vialard, J., Janicot, S., Cassou, C., Lengaigne, M., et al. (2017). Tropical explosive volcanic eruptions can trigger El Niño by cooling tropical Africa. *Nature Communications*, *8*(1), 1–13. https://doi.org/10.1038/s41467-017-00755-6

Krishnamurthy, L., & Krishnamurthy, V. (2014). Influence of PDO on South Asian summer monsoon and monsoon–ENSO relation. *Climate Dynamics*, *42*(9–10), 2397–2410. https://doi.org/10.1007/s00382-013-1856-z

Kucharski, F., Bracco, A., Yoo, J., Tompkins, A., Feudale, L., Ruti, P., & Dell'Aquila, A. (2009). A Gill-Matsuno-type mechanism explains the tropical Atlantic influence on African and Indian monsoon rainfall. *Quarterly Journal of the Royal Meteorological Society*, *135*(640), 569–579. https://doi.org/10.1002/qj.406

Kumar, K. K., Kleeman, R., Cane, M. A., & Rajagopalan, B. (1999). Epochal changes in Indian Monsoon-ENSO precursors. *Geophysical Research Letters*, *26*(1), 75–78. https://doi.org/10.1029/1998GL900226

Kumar, K. K., Rajagopalan, B., & Cane, M. A. (1999). On the weakening relationship between the Indian monsoon and ENSO. *Science*, *284*(5423), 2156–2159. https://doi.org/10.1126/science.284.5423.2156

Kumar, K. K., Rajagopalan, B., Hoerling, M., Bates, G., & Cane, M. (2006). Unraveling the mystery of Indian monsoon failure during El Niño. *Science*, *314*(5796), 115–119. https://doi.org/10.1126/science.1131152

Kumar, S., Phani, R., Mukhopadhyay, P., & Balaji, C. (2022). Does increasing horizontal resolution improve seasonal prediction of Indian summer monsoon? A climate forecast system model perspective. *Geophysical Research Letters*, *49*, e2021GL097466. https://doi.org/10.1029/2021GL097466

Landrum, L., Otto-Bliesner, B. L., Wahl, E. R., Conley, A., Lawrence, P. J., Rosenbloom, N., & Teng, H. (2013). Last millennium climate and its variability in CCSM4. *Journal of Climate*, *26*(4), 1085–1111. https://doi.org/10.1175/JCLI-D-11-00326.1

Lau, K., Kim, K., & Yang, S. (2000). Dynamical and boundary forcing characteristics of regional components of the Asian summer monsoon. *Journal of Climate*, *13*(14), 2461–2482. https://doi.org/10.1175/1520-0442(2000)013<2461:DABFCO>2.0.CO;2

Lee, J.-Y., & Wang, B. (2014). Future change of global monsoon in the CMIP5. *Climate Dynamics*, *42*(1), 101–119. https://doi.org/10.1007/s00382-012-1564-0

Li, X., & Ting, M. (2015). Recent and future changes in the Asian monsoon-ENSO relationship: Natural or forced? *Geophysical Research Letters*, *42*, 3502–3512. https://doi.org/10.1002/2015GL063557

Liu, B., Huang, G., Hu, K., Wu, R., Gong, H., Wang, P., & Zhao, G. (2018). The multidecadal variations of the interannual relationship between the East Asian summer monsoon and ENSO in a coupled model. *Climate Dynamics*, *51*(5–6), 1671–1686. https://doi.org/10.1007/s00382-017-3976-3

Liu, S., & Duan, A. (2017). Impacts of the leading modes of tropical Indian Ocean sea surface temperature anomaly on sub-seasonal evolution of the circulation and rainfall over East Asia during boreal spring and summer. *Journal of Meteorological Research*, *31*(1), 171–186. https://doi.org/10.1007/s13351-016-6093-z

Loo, Y. Y., Billa, L., & Singh, A. (2015). Effect of climate change on seasonal monsoon in Asia and its impact on the variability of monsoon rainfall in Southeast Asia. *Geoscience Frontiers*, *6*(6), 817–823. https://doi.org/10.1016/j.gsf.2014.02.009

Lu, R., Dong, B., & Ding, H. (2006). Impact of the Atlantic multidecadal oscillation on the Asian summer monsoon. *Geophysical Research Letters*, *33*, L24701. https://doi.org/10.1029/2006GL027655

Mantua, N. J., & Hare, S. R. (2002). The pacific decadal oscillation. *Journal of Oceanography*, *58*(1), 35–44. https://doi.org/10.1023/a:1015820616384

McMonigal, K., & Larson, S. M. (2022). Enso explains the link between Indian ocean dipole and meridional ocean heat transport. *Geophysical Research Letters*, *49*, e2021GL095796. https://doi.org/10.1029/2021GL095796

Mehta, V. M., & Lau, K.-M. (1997). Influence of solar irradiance on the Indian Monsoon-ENSO relationship at decadal-multidecadal time scales. *Geophysical Research Letters*, *24*(2), 159–162. https://doi.org/10.1029/96GL03778

Menon, A., Levermann, A., Schewe, J., Lehmann, J., & Frieler, K. (2013). Consistent increase in Indian monsoon rainfall and its variability across CMIP-5 models. *Earth System Dynamics*, *4*(2), 287–300. https://doi.org/10.5194/esd-4-287-2013

Midhun, M., Lekshmy, P. R., Thirumalai, K., & Ramesh, R. (2022). Coherent Indian Summer Monsoon and Sahel rainfall variability revealed by Ethiopian rainfall δ^{18}o. *Journal of Geophysical Research: Atmospheres*, *127*, e2022JD037160. https://doi.org/10.1029/2022JD037160

Mishra, V., Thirumalai, K., Singh, D., & Aadhar, S. (2020). Future exacerbation of hot and dry summer monsoon extremes in India. *npj Climate and Atmospheric Science*, *3*(1), 10. https://doi.org/10.1038/s41612-020-0113-5

Misios, S., Gray, L. J., Knudsen, M. F., Karoff, C., Schmidt, H., & Haigh, J. D. (2019). Slowdown of the Walker circulation at solar cycle maximum. *Proceedings of the National Academy of Sciences of the United States of America*, *116*(15), 7186–7191. https://doi.org/10.1073/pnas.1815060116

Muetzelfeldt, M. R., Schiemann, R., Turner, A. G., Klingaman, N. P., Vidale, P. L., & Roberts, M. J. (2021). Evaluation of Asian summer precipitation in different configurations of a high-resolution general circulation model in a range of decision-relevant spatial scales. *Hydrology and Earth System Sciences*, *25*(12), 6381–6405. https://doi.org/10.5194/hess-25-6381-2021

Nanjundiah, R. S., Francis, P. A., Ved, M., & Gadgil, S. (2013). Predicting the extremes of Indian summer monsoon rainfall with coupled ocean–atmosphere models. *Current Science*, *104*(10), 1380–1393.

Newman, M., Alexander, M. A., Ault, T. R., Cobb, K. M., Deser, C., Di Lorenzo, E., et al. (2016). The pacific decadal oscillation, revisited. *Journal of Climate*, *29*(12), 4399–4427. https://doi.org/10.1175/JCLI-D-15-0508.1

Otto-Bliesner, B. L., Brady, E. C., Fasullo, J., Jahn, A., Landrum, L., Stevenson, S., et al. (2016). Climate variability and change since 850 CE: An ensemble approach with the community Earth system model. *Bulletin of the American Meteorological Society*, *97*(5), 735–754. https://doi.org/10.1175/bams-d-14-00233.1

Parsons, L., & Hakim, G. (2019). Local regions associated with interdecadal global temperature variability in the Last Millennium Reanalysis and CMIP5 models. *Journal of Geophysical Research: Atmospheres*, *124*, 9905–9917. https://doi.org/10.1029/2019JD030426

Rajesh, P., & Goswami, B. (2022). A new emergent constraint corrected projections of Indian summer monsoon rainfall. *Geophysical Research Letters*, *49*, e2021GL096671. https://doi.org/10.1029/2021GL096671

Rani, S. I., Arulalan, T., George, J. P., Rajagopal, E. N., Renshaw, R., Maycock, A., et al. (2021). IMDAA: High-resolution satellite-era reanalysis for the Indian monsoon region. *Journal of Climate*, *34*(12), 5109–5133. https://doi.org/10.1175/JCLI-D-20-0412.1

Saranya, J., Roxy, M. K., Dasgupta, P., & Anand, A. (2022). Genesis and trends in marine heatwaves over the tropical Indian Ocean and their interaction with the Indian summer monsoon. *Journal of Geophysical Research: Oceans*, *127*, e2021JC017427. https://doi.org/10.1029/2021JC017427

Sarkar, S., & Maity, R. (2022). Future characteristics of extreme precipitation indicate the dominance of frequency over intensity: A multi-model assessment from CMIP6 across India. *Journal of Geophysical Research: Atmospheres*, *127*, e2021JD035539. https://doi.org/10.1029/2021JD035539

Schmidt, G. A., Jungclaus, J. H., Ammann, C. M., Bard, E., Braconnot, P., Crowley, T. J., et al. (2011). Climate forcing reconstructions for use in PMIP simulations of the last millennium (v1.0). *Geoscientific Model Development*, *4*(1), 33–45. https://doi.org/10.5194/gmd-4-33-2011

Schneider, U., Becker, A., Finger, P., Meyer-Christoffer, A., Rudolf, B., & Ziese, M. (2015). GPCC full data monthly product version 7.0 at 2.5°: Monthly land-surface precipitation from Rain-Gauges built on GTS-based and historic data [Dataset]. Global Precipitation Climatology Centre. https://doi.org/10.5676/DWD_GPCC/FD_M_V7_250

Schott, F. A., Xie, S.-P., & McCreary, J. P., Jr. (2009). Indian Ocean circulation and climate variability. *Reviews of Geophysics*, *47*, RG1002. https://doi.org/10.1029/2007RG000245

Singh, M., Krishnan, R., Goswami, B., Choudhury, A. D., Swapna, P., Vellore, R., et al. (2020). Fingerprint of volcanic forcing on the ENSO-Indian monsoon coupling. *Science Advances*, *6*(38), eaba8164. https://doi.org/10.1126/sciadv.aba8164

Sooraj, K. P., Terray, P., & Mujumdar, M. (2015). Global warming and the weakening of the Asian summer monsoon circulation: Assessments from the CMIP5 models. *Climate Dynamics*, *45*(1), 233–252. https://doi.org/10.1007/s00382-014-2257-7

Steiger, N. J. (2018). Paleo Hydrodynamics data assimilation product (PHYDA) [Dataset]. Zenodo. https://doi.org/10.5281/zenodo.1198817

Steiger, N. J., Hakim, G. J., Steig, E. J., Battisti, D. S., & Roe, G. H. (2014). Assimilation of time-averaged pseudoproxies for climate reconstruction. *Journal of Climate*, *27*(1), 426–441. https://doi.org/10.1175/JCLI-D-12-00693.1

Steiger, N. J., Smerdon, J. E., Cook, B. I., Seager, R., Williams, A. P., & Cook, E. R. (2019). Oceanic and radiative forcing of medieval megadroughts in the american southwest. *Science Advances*, *5*(7), eaax0087. https://doi.org/10.1126/sciadv.aax0087

Steiger, N. J., Smerdon, J. E., Cook, E. R., & Cook, B. I. (2018). A reconstruction of global hydroclimate and dynamical variables over the Common Era. *Scientific Data*, *5*(1), 180086. https://doi.org/10.1038/sdata.2018.86

Tao, S.-Y., & Chen, L.-X. (1987). A review of recent research on the East Asian summer monsoon in China. In *Monsoon meteorology* (pp. 60–92). Oxford University Press.

Tardif, R., Hakim, G. J., Perkins, W. A., Horlick, K. A., Erb, M. P., Emile-Geay, J., et al. (2019a). Last Millennium Reanalysis with an expanded proxy database and seasonal proxy modeling. *Climate of the Past*, *15*(4), 1251–1273. https://doi.org/10.5194/cp-15-1251-2019

Tardif, R., Hakim, G. J., Perkins, W. A., Horlick, K., Erb, M. P., Emile-Geay, J., et al. (2019b). NOAA/WDS Paleoclimatology—Last millennium reanalysis (LMR) project global climate reconstructions version 2 [Dataset]. NOAA National Centers for Environmental Information. https://doi.org/10.25921/gn22-5866

Tejavath, C. T., Ashok, K., Chakraborty, S., & Ramesh, R. (2019). A PMIP3 narrative of modulation of ENSO teleconnections to the Indian summer monsoon by background changes in the Last Millennium. *Climate Dynamics*, *53*(5–6), 3445–3461. https://doi.org/10.1007/s00382-019-04718-z

Torrence, C., & Webster, P. J. (1999). Interdecadal changes in the ENSO-monsoon system. *Journal of Climate*, *12*(8), 2679–2690. https://doi.org/10.1175/1520-0442(1999)012<2679:ICITEM>2.0.CO;2

Wang, B., & Fan, Z. (1999). Choice of South Asian summer monsoon indices. *Bulletin of the American Meteorological Society*, *80*(4), 629–638. https://doi.org/10.1175/1520-0477(1999)080<0629:COSASM>2.0.CO;2

Wang, B., Wu, R., & Lau, K. (2001). Interannual variability of the Asian summer monsoon: Contrasts between the Indian and the western north pacific–East Asian monsoons. *Journal of Climate*, *14*(20), 4073–4090. https://doi.org/10.1175/1520-0442(2001)014<4073:IVOTAS>2.0.CO;2

Wang, B., Wu, R., & Li, T. (2003). Atmosphere-warm ocean interaction and its impacts on Asian-Australian monsoon variation. *Journal of Climate*, *16*(8), 1195–1211. https://doi.org/10.1175/1520-0442(2003)16<1195:AOIAII>2.0.CO;2

Wang, B., Wu, Z., Li, J., Liu, J., Chang, C.-P., Ding, Y., & Wu, G. (2008). How to measure the strength of the East Asian summer monsoon. *Journal of Climate*, *21*(17), 4449–4463. https://doi.org/10.1175/2008JCLI2183.1

Wang, H. (2002). The instability of the East Asian summer monsoon-ENSO relations. *Advances in Atmospheric Sciences*, *19*(1), 1–11. https://doi.org/10.1007/s00376-002-0029-5

Wang, Y., Ren, H.-L., Wei, Y., Jin, F.-F., Ren, P., Gao, L., & Wu, J. (2022). MJO Phase swings modulate the recurring latitudinal shifts of the 2020 extreme summer-monsoon rainfall around Yangtse. *Journal of Geophysical Research: Atmospheres*, *127*, e2021JD036011. https://doi.org/10.1029/2021JD036011

Wen, Q., Yan, M., Liu, Z., & Liu, J. (2022). Responses of East Asian winter monsoon-Australian summer monsoon to local and remote orbital forcing during Holocene. *Geophysical Research Letters*, *49*, e2022GL098865. https://doi.org/10.1029/2022GL098865

Wu, R., & Wang, B. (2002). A contrast of the East Asian summer monsoon-ENSO relationship between 1962–77 and 1978–93. *Journal of Climate*, *15*(22), 3266–3279. https://doi.org/10.1175/1520-0442(2002)015<3266:ACOTEA>2.0.CO;2

Wu, Z., Li, J., Jiang, Z., He, J., & Zhu, X. (2012). Possible effects of the North Atlantic oscillation on the strengthening relationship between the East Asian summer monsoon and ENSO. *International Journal of Climatology*, *32*(5), 794–800. https://doi.org/10.1002/joc.2309

Wu, Z., Li, J., Jiang, Z., & Ma, T. (2012). Modulation of the Tibetan Plateau snow cover on the ENSO teleconnections: From the East Asian summer monsoon perspective. *Journal of Climate*, *25*(7), 2481–2489. https://doi.org/10.1175/JCLI-D-11-00135.1

Xie, S.-P., Annamalai, H., Schott, F. A., & McCreary, J. P., Jr. (2002). Structure and mechanisms of South Indian Ocean climate variability. *Journal of Climate*, *15*(8), 864–878. https://doi.org/10.1175/1520-0442(2002)015<0864:SAMOSI>2.0.CO;2

Xie, S.-P., Hu, K., Hafner, J., Tokinaga, H., Du, Y., Huang, G., & Sampe, T. (2009). Indian Ocean capacitor effect on Indo-western Pacific climate during the summer following El Niño. *Journal of Climate*, *22*(3), 730–747. https://doi.org/10.1175/2008JCLI2544.1

Xie, S.-P., Kosaka, Y., Du, Y., Hu, K., Chowdary, J. S., & Huang, G. (2016). Indo-western Pacific Ocean capacitor and coherent climate anomalies in post-ENSO summer: A review. *Advances in Atmospheric Sciences*, *33*(4), 411–432. https://doi.org/10.1007/s00376-015-5192-6

Yan, H., Wei, W., Soon, W., An, Z., Zhou, W., Liu, Z., et al. (2015). Dynamics of the intertropical convergence zone over the western pacific during the little ice age. *Nature Geoscience*, *8*(4), 315–320. https://doi.org/10.1038/ngeo2375

Yun, K.-S., & Timmermann, A. (2018). Decadal monsoon-ENSO relationships reexamined. *Geophysical Research Letters*, *45*, 2014–2021. https://doi.org/10.1002/2017GL076912

Zhang, D. (1991). Historical records of climate change in China. *Quaternary Science Reviews*, *10*(6), 551–554. https://doi.org/10.1016/0277-3791(91)90049-Z

Zhang, X., Wu, M., Liu, Y., Hao, Z., & Zheng, J. (2018). The relationship between the East Asian summer monsoon and El Niño-southern oscillation revealed by reconstructions and a control simulation for millennium. *Quaternary International*, *493*, 106–113. https://doi.org/10.1016/j.quaint.2018.06.024

Zhang, Y., Zhou, W., Wang, X., Chen, S., Chen, J., & Li, S. (2022). Indian Ocean Dipole and ENSO's mechanistic importance in modulating the ensuing-summer precipitation over Eastern China. *npj Climate and Atmospheric Science*, *5*(1), 48. https://doi.org/10.1038/s41612-022-00271-5

Zhou, Z.-Q., Xie, S.-P., & Zhang, R. (2021). Historic Yangtze flooding of 2020 tied to extreme Indian Ocean conditions. *Proceedings of the National Academy of Sciences of the United States in America*, *118*, e2022255118. https://doi.org/10.1073/pnas.2022255118